IEEE Open Journal of
Power Electronics

Received 2 December 2022; accepted 29 December 2022. Date of publication 6 January 2023;
date of current version 30 January 2023. The review of this article was arranged by Associate Editor Xiaoqing Song.

Digital Object Identifier 10.1109/OJPEL.2023.3234803

Stability and Sensitivity Analysis of Multi-Vendor, Multi-Terminal HVDC Systems

YICHENG LIAO [1,2] (Member, IEEE), HENG WU [1] (Member, IEEE), XIONGFEI WANG [1,2] (Fellow, IEEE), MARIO NDREKO[3], ROBERT DIMITROVSKI[3], AND WILHELM WINTER[3]

[1]AAU Energy, Aalborg University, 9220 Aalborg, Denmark
[2]Division of Electric Power and Energy Systems, KTH Royal Institute of Technology, 10044 Stockholm, Sweden
[3]Electrical System Design, TenneT TSO GmbH, 95448 Bayreuth, Germany

CORRESPONDING AUTHOR: XIONGFEI WANG (e-mail: xiongfei@kth.se)

This work was financed by TenneT TSO GmbH.

ABSTRACT Multi-terminal HVDC projects are increasingly developed in recent years to enhance the flexibility of energy transmission. Differing from the point-to-point HVDC systems, it is more challenging to design the multi-terminal HVDC system and ensure stable interoperability among converter systems, especially when the converters are manufactured from different vendors. Although impedance-based stability analysis allows for analyzing such systems based on black-box models, it is still difficult to utilize those black-box models to identify the root cause of potential instability. To tackle this challenge, this paper proposes a multi-level sensitivity analysis approach using frequency-domain sensitivity functions based on the impedance-based stability criterion. The proposed method differs from the classical sensitivity analysis based on state-space or transfer-function models, as it is purely based on black-box impedance models. Case studies on a four-terminal HVDC system are carried out for stability and sensitivity analysis based on the impedance measurement in PSCAD, through which the most sensitive HVDC station can be identified. The proposed theory and the analyzed results are finally validated by electromagnetic transient simulations.

INDEX TERMS Impedance stability, multi-terminal HVDC system, black-box system, sensitivity analysis, frequency-domain analysis.

NOMENCLATURE

PoC	Point of connection.
MIMO	Multi-input and multi-output.
s	Complex variable for Laplace transform.
ω	Angular frequency for frequency-domain analysis.

Transfer functions or variables (all can be functions of s or ω):

$\mathbf{Y}_{\text{st}}$	Total admittance matrix of all MMC stations at multiple PoCs.
$\mathbf{Y}_{\text{net}}$ ($\mathbf{Z}_{\text{net}}$)	Total admittance (impedance) matrix of the passive network at multiple PoCs.
$\mathbf{Y}_m$	Admittance matrix of the m-th MMC station at its own PoCs.
$Z_{p,m}$	Positive-pole impedance of the m-th MMC station.
$Z_{n,m}$	Negative-pole impedance of the m-th MMC station.
$\mathbf{Y}_{\text{cable}m}$	Admittance matrix of the m-th cable at its own PoCs.
V_k	Voltage at the k-th port.
I_k	Current flowing from the MMC station to the network at the k-th port.
$\mathbf{L}$	Return ratio of a MIMO system.
l_{ij}	i-th row, j-th column element of $\mathbf{L}$.
$\mathbf{F}$	Return difference of a MIMO system.
$\mathbf{\Lambda}$	Eigenvalue matrix of $\mathbf{L}$.
λ_i	i-th eigenvalue of $\mathbf{L}$.
$\mathbf{W}$	Left eigenvector matrix of $\mathbf{L}$.
w_{ij}	i-th row, j-th column element of $\mathbf{W}$.
$\mathbf{V}$	Right eigenvector matrix of $\mathbf{L}$.
v_{ki}	k-th row, i-th column element of $\mathbf{V}$.
$S_x^y = \frac{\partial y}{\partial x}$	Sensitivity function of y with respect to x, where x and y apply for any variables.

Constant matrices or numbers:

E	Unity matrix.
O	Zero matrix.
P	Number of open-loop right-half-plane poles of a MIMO system.
N	Total number of anticlockwise encirclements around $(-1, 0)$ on Nyquist diagrams of all λ_i.

I. INTRODUCTION

Power electronic converters play important roles in high-voltage direct-current (HVDC) transmission systems for efficient and flexible power supply. The HVDC technology has been applied for point-to-point interconnections for more than half a century. Until recently, the needs for utilizing HVDC for multi-terminal interconnections have been increasingly identified in more hybrid projects, such as North Sea Wind Power Hub [1]. However, due to the fast dynamics of converter's control, the interactions among power converters and power grids can lead to oscillations in a wide frequency range [2], [3], which could jeopardize the power quality and may even threaten the stable operation of the power system if converters trip.

In order to enable the development of future multi-terminal HVDC systems, the interoperability of multi-vendor projects has to be ensured in the planning and design phase [4], [5]. It is usually the responsibility of transmission system operators (TSOs) or if applicable the owner of such HVDC systems to conduct together with the HVDC suppliers a system-level stability assessment to prove that HVDC converters can be connected at the DC side without interoperability risks of its control systems. To assess the control-induced stability of a multi-vendor multi-terminal HVDC system, the common practice is to run electromagnetic transient (EMT) simulations either on offline or real-time platforms [3], [6]. Although, the EMT simulation is the safest way to prove the stability of the overall system as it contains detailed modelling up to component level, it cannot provide sufficient insights to the instability mechanisms taking placed when adverse interactions are observed. As a consequence, a lot of research works have been carried out in recent years on the dynamical modeling and analysis of HVDC systems [7], [8], [9], [10]. Among the existing studies, the impedance-based approach [7], [10] becomes more and more attractive since it can capture the frequency behavior of the converters at their connection points, and at the same time the study can be performed while respecting the intellectual property of the HVDC manufacturers. The dynamic behaviors of such converters can be characterized by impedance models at their points of connection (PoCs) through frequency-scan measurement performed on an EMT simulation platform, then the system stability can be further assessed by the frequency-domain tools. This approach also provides some insights into the instability mechanism, that is the negative resistance caused by converter controls can cause instability issues when interacting with grid impedances [11]. However, most of the studies using impedance-based analysis still focus on the converter control interactions for a point-to-point connection.

When multiple converters are interconnected to each other through complex networks, especially for the multi-vendor multi-terminal HVDC systems, the interoperability of converters becomes more complicated, since multiple converters may introduce negative resistance which can interact with each other through meshed networks. In such cases, it is more challenging to identify the role of each converter in the overall stability at the system level. A few recent publications have studied the stability and sensitivity of multi-converter based systems using impedance models [12], [13], [14]. There are two major approaches. One is based on the pole-residue relationship of transfer functions, where the sensitivity of the system oscillation modes with respect to impedance models is derived to characterize the impacts of nodal voltages or branch currents on the system stability [12]. Furthermore, the parameter sensitivity can be deduced based on the chain rule if the sensitivity of impedance models with respect to any parameter is known [13]. However, this method requires pre-known s-domain transfer functions for the pole and residue calculation, which are usually not accessible for black-box systems. The other approach is based on the frequency-domain sensitivity functions, which is adopted in [14] to perform the sensitivity analysis of a multi-terminal HVDC system. The sensitivity functions of the determinant of the system return-difference matrix with respect to impedance models are derived to characterize the converters' impacts on the system stability. However, this approach relies on the assumption that the converter admittance models do not have right-half-plane poles. Thus, additional model modifications are needed when the assumption does not hold, which complicates the analysis. Furthermore, the DC network is only regarded as a single-port network for each converter station, which does not apply to the case where the station includes both positive and negative poles at the DC side. Another work develops a frequency-domain participation function to study the participation of converter systems into the system stability [15]. Actually, this approach is also equivalent to the frequency-domain sensitivity analysis, however, how to extend it for further-level sensitivity analysis and thus contribute to a system-level design has not been investigated by [15].

To address the aforementioned challenges, a multi-level sensitivity analysis approach is proposed to study the stability and sensitivity of multi-vendor, multi-terminal HVDC systems. Based on the multi-input multi-output (MIMO) impedance-based stability analysis using generalized Nyquist stability criterion (GNSC), multi-level sensitivity functions of the return-ratio eigenlocus are derived, which are combined with the stability analysis results to identify the root cause of potential instability. The proposed method differs from the prior art in the following aspects:

- Differing from the classical modal-based sensitivity analysis using state-space models (known **A, B, C, D**) or transfer function models (known s-domain functions) [12], [13], the proposed method is derived based on

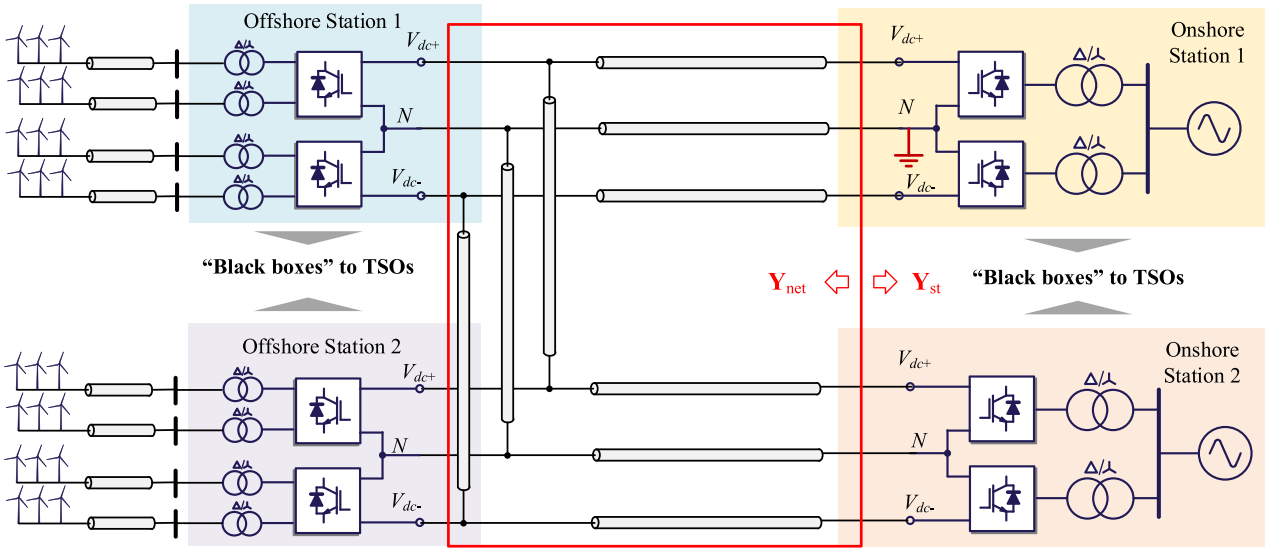

FIGURE 1. Four-terminal MMC-HVDC system under study.

frequency-domain sensitivity functions (only ω-domain functions). It can thus be directly applied for black-box systems.

- This work develops sensitivity functions based on the eigenlocus of the return ratio of a MIMO system, while [14] develops the sensitivity function based on the determinant of the return difference of a MIMO system. Thus, the sensitivity functions used in this work have lower transfer function orders, which are simpler in calculation.
- Compared with [15], the proposed method reveals that the sensitivity functions can be derived at different levels, which can thus be passed further down to lower levels in black-box forms. This brings potential solutions to practically addressing the converter interoperability among multi-vendor projects.

In the rest of the paper, Section II introduces the system under study and reviews the basic impedance-based stability criterion as the background. Section III proposes the multi-level sensitivity analysis approach and elaborates how it can benefit to system-level studies. Section IV provides the case studies based on measured impedance models in EMT simulations. Conclusions and prospects are summarized in Section V.

II. FUNDAMENTALS OF IMPEDANCE-BASED ANALYSIS

A. SYSTEM DESCRIPTION AND ASSUMPTIONS

Fig. 1 shows an offshore four-terminal HVDC system under study, which is based on modular multi-level converters (MMCs). Two onshore stations and two offshore stations are connected through HVDC cables. The onshore stations are controlled in the grid-following mode, while the offshore stations are controlled in the grid-forming mode (applying V/f control). There are two assumptions considered in this work:

- The MMC HVDC stations are manufactured by different vendors, thus, their control algorithms are encrypted, and they can only be treated as black-box models for the system-level study.
- The impedance models are used to characterize the system dynamic behaviors, which can be obtained through impedance measurement obtained from EMT simulation platforms [16], [17].

B. ADMITTANCE FORMULATION

To conduct the impedance-based stability analysis, the entire system is partitioned into one active subsystem and one passive subsystem by multiple points of connection (PoCs) [15], [18], [19] as shown by the red box in Fig. 1. Outside the red box is the active subsystem including all the MMC stations, whose admittance model can be represented by $\mathbf{Y}_{st}$. Inside the red box is the passive subsystem composed by the DC network, whose admittance model is denoted by $\mathbf{Y}_{net}$.

Through the subsystem partition, the entire system can be treated as a multi-port cascaded system, as shown in Fig. 2. Differing from the studies for AC system interconnections in [15], [18], [19], each MMC station has a positive pole and a negative pole, whose dynamics need to be represented by two DC impedances. Thus, each MMC station is regarded as a three-port system at the PoCs. Any DC cable among two MMC stations can be represented by a six-port system. The four-terminal HVDC system is thus represented as a twelve-port cascaded system.

The sequence of the PoCs is denoted by k, varying from 1 to 12. Then, the k-th port voltage is defined by V_k. The k-th port current flowing from the MMC to the DC network is defined as I_k. Thus, the MMC station admittance can be derived as

$$\mathbf{Y}_{st} = \begin{bmatrix} \mathbf{Y}_1 & & & \\ & \mathbf{Y}_2 & & \\ & & \mathbf{Y}_3 & \\ & & & \mathbf{Y}_4 \end{bmatrix}. \tag{1}$$

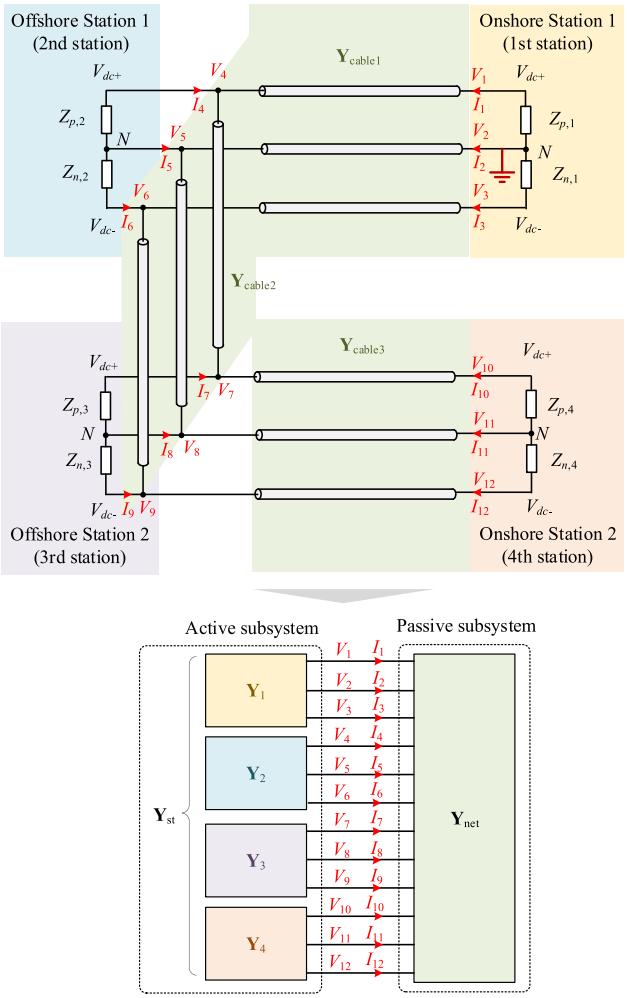

FIGURE 2. Subsystem partition for admittance representation.

where $\mathbf{Y}_1, \mathbf{Y}_2, \mathbf{Y}_3, \mathbf{Y}_4$ represent the admittance matrices of the Onshore Station 1, Offshore Station 1, Offshore Station 2, and Onshore Station 2, respectively.

Without losing generality, each MMC station admittance can be denoted by its positive-pole and negative-pole impedances, as shown in Fig. 2. The subscript 'p' or 'n' denotes the positive or negative pole, and the subscript of number denotes the station sequential number. For each station, it is a three-port network; thus, based on the terminal current and voltage relationships, the m-th station admittance matrix can be deduced as

$$\mathbf{Y}_m = \begin{bmatrix} \frac{1}{Z_{p,m}} & -\frac{1}{Z_{p,m}} & \\ -\frac{1}{Z_{p,m}} & \frac{1}{Z_{p,m}} + \frac{1}{Z_{n,m}} & -\frac{1}{Z_{n,m}} \\ & -\frac{1}{Z_{n,m}} & \frac{1}{Z_{n,m}} \end{bmatrix}. \tag{2}$$

where $Z_{p,m}$ is the positive-pole impedance and $Z_{n,m}$ is the negative-pole impedance.

It is assumed that each cable admittance is represented by $\mathbf{Y}_{\text{cable}k}$, which should be a six-by-six matrix according to the number or PoCs. Then, based on the cable configurations among the defined ports, the DC network admittance can be

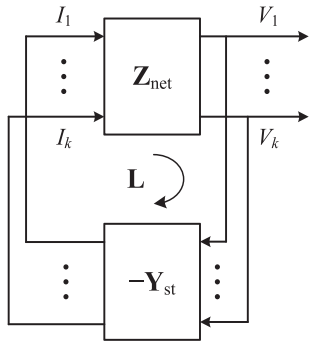

FIGURE 3. Loop gain representation of the multi-port interconnected system using impedance models.

deduced as

$$\mathbf{Y}_{\text{net}} = \begin{bmatrix} \square & \square & \mathbf{O} & \mathbf{O} \\ \square & \square & \mathbf{O} & \mathbf{O} \\ \mathbf{O} & \mathbf{O} & \mathbf{O} & \mathbf{O} \\ \mathbf{O} & \mathbf{O} & \mathbf{O} & \mathbf{O} \end{bmatrix}_{\mathbf{Y}_{\text{cable1}}} + \begin{bmatrix} \mathbf{O} & \mathbf{O} & \mathbf{O} & \mathbf{O} \\ \mathbf{O} & \square & \square & \mathbf{O} \\ \mathbf{O} & \square & \square & \mathbf{O} \\ \mathbf{O} & \mathbf{O} & \mathbf{O} & \mathbf{O} \end{bmatrix}_{\mathbf{Y}_{\text{cable2}}} + \begin{bmatrix} \mathbf{O} & \mathbf{O} & \mathbf{O} & \mathbf{O} \\ \mathbf{O} & \mathbf{O} & \mathbf{O} & \mathbf{O} \\ \mathbf{O} & \mathbf{O} & \square & \square \\ \mathbf{O} & \mathbf{O} & \square & \square \end{bmatrix}_{\mathbf{Y}_{\text{cable3}}} \tag{3}$$

where $\mathbf{O}$ or $\square$ represents a three-by-three block matrix. $\mathbf{O}$ denotes a zero matrix and $\square$ denotes a non-zero matrix. It can be seen that $\mathbf{Y}_{\text{cable1}}$ is associated to the Ports 1-6, since it connects the Onshore Station 1 and the Offshore Station 1. $\mathbf{Y}_{\text{cable2}}$ is associated to the Ports 4-9, since it connects the Offshore Station 1 and the Offshore Station 2. $\mathbf{Y}_{\text{cable3}}$ is associated to the Ports 7-12, since it connects the Offshore Station 2 and the Onshore Station 2.

C. IMPEDANCE-BASED STABILITY CRITERION

The interconnected system in Fig. 2 can be formulated by a multivariable feedback control system, with the loop gain representation shown in Fig. 3. It is noted that only $\mathbf{Y}_{\text{net}}$ can be inversed as $\mathbf{Z}_{\text{net}}$, and $\mathbf{Y}_{\text{st}}$ cannot be inversed, since (2) has the rank of two.

Then, the system return ratio is defined as

$$\mathbf{L}(s) = \mathbf{Y}_{\text{st}}(s)\,\mathbf{Z}_{\text{net}}(s) \tag{4}$$

and the system return difference is defined as

$$\mathbf{F}(s) = \mathbf{E} + \mathbf{L}(s) \tag{5}$$

where $\mathbf{E}$ is an identity matrix.

The stability of a multivariable feedback system can be analyzed by the GNSC [20], which in general includes three steps:

- *Step 1:* Identify the number of open-loop right-half-plane (RHP) poles (P) by the poles of $\det(\mathbf{F}(s))$, as the system's open-loop characteristic polynomial can be determined by the denominator polynomial of $\det(\mathbf{F}(s))$ [20]. In practice, for black-box systems, the pole information can also be judged from observations on the Bode diagram of $\det(\mathbf{F}(\omega))$, where a RHP pole can result in a magnitude

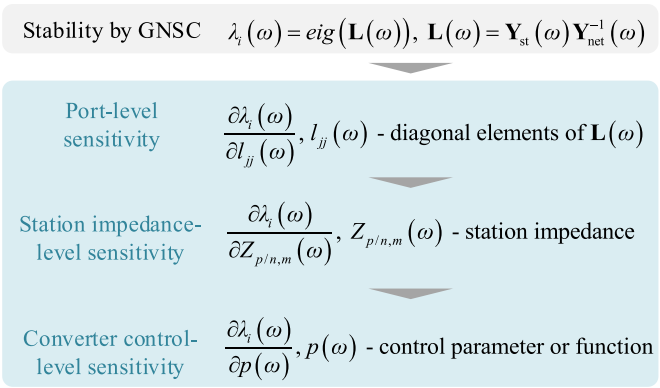

FIGURE 4. Multi-level sensitivity analysis using different sensitivity functions.

decrease and a phase increase as the frequency increases [21].

- *Step 2:* Count the total number of anticlockwise encirclements (N) around (-1, 0) on Nyquist diagrams of $\lambda_i(s)$, where $\lambda_i(s)$ for all i are the eigenvalues of $\mathbf{L}(s)$.
- *Step 3:* Check the stability by judging if $P = N$.

It can be seen that the system stability is influenced significantly by the eigenloci of $\mathbf{L}(s)$, thus, the system sensitivity can be analyzed in the frequency domain based on sensitivity functions of $\lambda_i(s)$.

III. MULTI-LEVEL SENSITIVITY ANALYSIS

A multi-level sensitivity analysis approach is proposed in this section based on the frequency-domain sensitivity theory [22]. According to the GNSC, the trajectory of $\lambda_i(s)$ affects the stability significantly. Thus, the sensitivity analysis can be conducted by deriving sensitivity functions of $\lambda_i(s)$ with respect to any other transfer function $G(s)$ of interest, i.e.,

$$\begin{aligned} S_G^{\lambda_i}(s) &= \partial\lambda_i(s)/\partial G(s) \\ &\downarrow \text{ frequency domain} \\ S_G^{\lambda_i}(\omega) &= \partial\lambda_i(\omega)/\partial G(\omega) \end{aligned} \tag{6}$$

Eq. (6) can be derived analytically in s domain. It can also be derived in the frequency domain based on frequency scans of black-box systems, since s can be substituted by $j\omega$, and $\lambda_i(\omega)$ and $G(\omega)$ can also be calculated at each frequency point. To highlight the sensitivity function is a frequency-domain method, the following transfer functions are represented in ω domain instead of s domain.

The frequency-domain sensitivity function in (6) allows for doing sensitivity analysis at different levels, depending on which $G(\omega)$ is of interest. A multi-level sensitivity analysis approach is then developed in Fig. 4. The sensitivity can be analyzed at the port level, station impedance level, and the converter control level, which are introduced in Parts A-C. Since the sensitivity function used here is not identical to the classical modal-based sensitivity, which is a scaler, the sensitivity analysis shall be interpreted in the frequency domain, which is further introduced in Part D. Part E finally discusses the comparison between the proposed sensitivity method with the existing sensitivity methods.

A. PORT-LEVEL SENSITIVITY

The port-level sensitivity quantifies the impacts of different port voltages/currents on the eigenlocus $\lambda_i(\omega)$.

According to Fig. 3, there exists

$$[\mathbf{E}+\mathbf{L}(\omega)]\begin{bmatrix} I_1 & \cdots & I_k \end{bmatrix}^{\mathrm{T}} = \mathbf{0} \tag{7}$$

Thus, the return ratio $\mathbf{L}(\omega) = \mathbf{Y}_{st}(\omega)\mathbf{Z}_{net}(\omega)$ denotes how the port currents affect their owns through the entire feedback loop. Similarly, if $\mathbf{L}(\omega)$ is defined as $\mathbf{Z}_{net}(\omega)\mathbf{Y}_{st}(\omega)$, it denotes how the port voltages affect their owns through the entire feedback loop.

Through the eigenvalue decomposition, $\mathbf{L}(\omega)$ can be represented by the eigenvalue matrix and the eigenvector matrices, i.e.,

$$\begin{aligned} &\mathbf{L}(\omega) = \mathbf{V}(\omega)\,\mathbf{\Lambda}(\omega)\,\mathbf{W}(\omega) \\ &\text{where } \mathbf{V}(\omega) - \text{right eigenvector matrix} \\ &\qquad \mathbf{\Lambda}(\omega) - \text{eigenvalue matrix} \\ &\qquad \mathbf{W}(\omega) - \text{left eigenvector matrix} \end{aligned} \tag{8}$$

Then, the sensitivity function of $\lambda_i(\omega)$ with respect to $l_{jk}(\omega)$ can be derived as

$$S_{l_{jk}}^{\lambda_i}(\omega) = \frac{\partial\lambda_i(\omega)}{\partial l_{jk}(\omega)} = w_{ij}(\omega)\,v_{ki}(\omega) \tag{9}$$

where $\lambda_i(\omega)$ – the i-th diagonal element of $\mathbf{\Lambda}(\omega)$
$l_{jk}(\omega)$ – the j-th row, k-th column element of $\mathbf{L}(\omega)$
$w_{ij}(\omega)$ – the i-th row, j-th column element of $\mathbf{W}(\omega)$
$v_{ki}(\omega)$ – the k-th row, i-th column element of $\mathbf{V}(\omega)$

The detailed proof of (9) is presented in Appendix-A. It is noted that this sensitivity function can be calculated directly from the left and right eigenvector matrices. Therefore, even though $\mathbf{L}(\omega)$ is a black-box system, the sensitivity function can still be calculated based on $\mathbf{W}(\omega)$ and $\mathbf{V}(\omega)$ at each frequency points.

If it is assumed that $j = k$ in (9), it calculates the eigenlocus sensitivity functions with respect to diagonal elements of $\mathbf{L}(\omega)$. Considering all eigenloci and all diagonal elements, a sensitivity matrix can be formulated as

$$\begin{aligned} &\mathbf{P}(\omega) := \begin{bmatrix} S_{l_{11}}^{\lambda_1}(\omega) & \cdots & S_{l_{11}}^{\lambda_i}(\omega) \\ \vdots & \ddots & \vdots \\ S_{l_{jj}}^{\lambda_1}(\omega) & \cdots & S_{l_{jj}}^{\lambda_i}(\omega) \end{bmatrix} \\ &\text{where } S_{l_{jj}}^{\lambda_i}(\omega) = \frac{\partial\lambda_i(\omega)}{\partial l_{jj}(\omega)} = w_{ij}(\omega)\,v_{ji}(\omega) \end{aligned} \tag{10}$$

It can be found that the sensitivity functions in (10) is essentially the same as the participation functions defined in [15]. Thus, the sensitivity at this level only considering diagonal elements of $\mathbf{L}(\omega)$ can also be named as port-level sensitivity or port participation analysis.

The derivation of the port participation function is similar to the state participation factor for state-space analysis [23],

where the sum of each row or column is equal to one. However, the implication here is different. The state participation factor is merely a scaler, while the port participation function in (10) is a function of ω.

B. STATION IMPEDANCE-LEVEL SENSITIVITY

The port participation function only analyzes the eigenlocus sensitivity with respect to the diagonal elements of $\mathbf{L}(\omega)$. The off-diagonal elements of $\mathbf{L}(\omega)$ also affect the eigenloci, which is not considered in the port participation analysis. To consider the sensitivity impacts from the off-diagonal elements of $\mathbf{L}(\omega)$, sensitivity analysis can be done further at the station impedance level. This can be realized by deriving the sensitivity functions of $\lambda_i(\omega)$ with respect to the station impedance $Z_{p/n,m}(\omega)$, where the subscript "*p/n*" denotes the positive-pole or negative-pole impedance, and the subscript "*m*" denotes the *m*-th station.

Since (9) only reveals how the elements of $\mathbf{L}(\omega)$ affect the eigenlocus, it is still unclear how the station impedance affects the off-diagonal elements of $\mathbf{L}(\omega)$ and even further affects the eigenlocus. Therefore, the sensitivity function matrix of $\mathbf{L}(\omega)$ with respect to $Z_{p/n,m}(\omega)$ needs to be also considered, which can be derived as

$$\begin{aligned}\mathbf{S}^{\mathbf{L}}_{Z_{p/n,m}}(\omega) &:= \frac{\partial \mathbf{L}(\omega)}{\partial Z_{p/n,m}(\omega)} = \frac{\partial \mathbf{Y}_{\text{st}}(\omega)}{\partial Z_{p/n,m}(\omega)}\mathbf{Z}_{\text{net}}(\omega) \\ &= \begin{bmatrix} \frac{\partial \mathbf{Y}_1(\omega)}{\partial Z_{p/n,m}(\omega)} & & & \\ & \ddots & & \\ & & \frac{\partial \mathbf{Y}_k(\omega)}{\partial Z_{p/n,m}(\omega)} & \\ & & & \ddots \end{bmatrix} \mathbf{Z}_{\text{net}}(\omega)\end{aligned} \tag{11}$$

where $\mathbf{Y}_k(\omega)$ represents the *k*-th station admittance matrix at its PoCs, according to (1).

It is worth noting that for all $k \neq m$, $\frac{\partial \mathbf{Y}_k(\omega)}{\partial Z_{p/n,m}(\omega)}$ is a zero matrix, since the *k*-th station admittance matrix $\mathbf{Y}_k(\omega)$ is irrelevant to the *m*-th station impedance $Z_{p/n,m}(\omega)$. When $k = m$ $\frac{\partial \mathbf{Y}_m(\omega)}{\partial Z_{p/n,m}(\omega)}$ can be derived according to (2). The detailed proof of (11) is presented in Appendix-B.

Then, combining (9) and (11), according to the chain rule, the sensitivity function of $\lambda_i(\omega)$ with respect to $Z_{p/n,m}(\omega)$ can be derived as

$$\begin{aligned}&S^{\lambda_i}_{Z_{p/n,m}}(\omega) = \frac{\partial \lambda_i(\omega)}{\partial Z_{p/n,m}(\omega)} = \sum_{j,k} S^{\lambda_i}_{l_{jk}}(\omega) S^{l_{jk}}_{Z_{p/n,m}}(\omega) \\ &\text{where } S^{l_{jk}}_{Z_{p/n,m}}(\omega) \text{ is the } j-\text{th row}, k-\text{th column} \\ &\text{element of } \mathbf{S}^{\mathbf{L}}_{Z_{p/n,m}}(\omega)\end{aligned} \tag{12}$$

The eigenloci and station impedances can have different magnitudes. To compare the eigenlocus sensitivity functions with respect to different station impedances, the sensitivity function of (12) can be normalized as

$$S^{\lambda_i}_{Z_{p/n,m}}(\omega) = \frac{Z_{p/n,m}(\omega)}{\lambda_i(\omega)} \sum_{j,k} S^{\lambda_i}_{l_{jk}}(\omega) S^{l_{jk}}_{Z_{p/n,m}}(\omega) \tag{13}$$

C. CONVERTER CONTROL-LEVEL SENSITIVITY

According to the chain rule, the sensitivity can be done further down to the converter control level, if the sensitivity function of $Z_{p/n,m}(\omega)$ with respect to any converter control parameter or function of $p(\omega)$ is known. Then, the eigenlocus sensitivity can be derived as

$$S^{\lambda_i}_{p}(\omega) = \frac{\partial \lambda_i(\omega)}{\partial p(\omega)} = \frac{\partial \lambda_i(\omega)}{\partial Z_{p/n,m}(\omega)} \cdot \frac{\partial Z_{p/n,m}(\omega)}{\partial p(\omega)} \tag{14}$$

In (14), the station impedance level sensitivity $\frac{\partial \lambda_i(\omega)}{\partial Z_{p/n,m}(\omega)}$ can be provided by TSOs, since the network work information and black-box station impedance models are known by TSOs. $\frac{\partial Z_{p/n,m}(\omega)}{\partial p(\omega)}$ may not be available information for TSOs, since the converter control details are kept confidential by converter manufacturers. However, the converter manufacturers know their control details, so they are able to derive the analytical model of $Z_{p/n,m}(\omega)$ and its sensitivity function with any $p(\omega)$ of interest. The multi-level sensitivity analysis approach proves that the sensitivity functions can be transferred from the system level to the converter level. Thus, it provides potentials for converter manufacturers to use the upper-level black-box sensitivity functions, i.e., $\frac{\partial \lambda_i(\omega)}{\partial Z_{p/n,m}(\omega)}$, for the bottom-level sensitivity analysis, which can benefit to the converter control design to optimize the system stability.

D. SENSITIVITY INTERPRETATION BASED ON STABILITY ANALYSIS

The previous sections have defined the sensitivity functions for analysis at different levels. These functions need to be further analyzed and interpreted based on the frequency-domain stability analysis. This can be realized by following the steps below:

- *Step 1:* Find the critical eigenloci that affect the stability significantly and identify the critical frequency range where the potential instability may happen.
  The critical eigenloci are the ones close to $(-1, 0)$ on the Nyquist diagram, since their encirclements around $(-1, 0)$ are more likely to be changed with system parameter change, which are thus more sensitive to the system stability. The critical frequency range should be the neighborhood where the Nyquist diagram is close to $(-1, 0)$, which can be identified on the Bode diagram. The critical frequency range is usually around the magnitude crossover frequency of 0 dB or the phase crossover frequency of 180°.
- *Step 2:* Calculate the critical eigenlocus sensitivity functions and compared their magnitude responses in the critical frequency range.
  At the port level, the port participation analysis can be conducted for the critical eigenloci. In the critical frequency range, the ports with highest participations should take dominant roles in the system stability or instability.

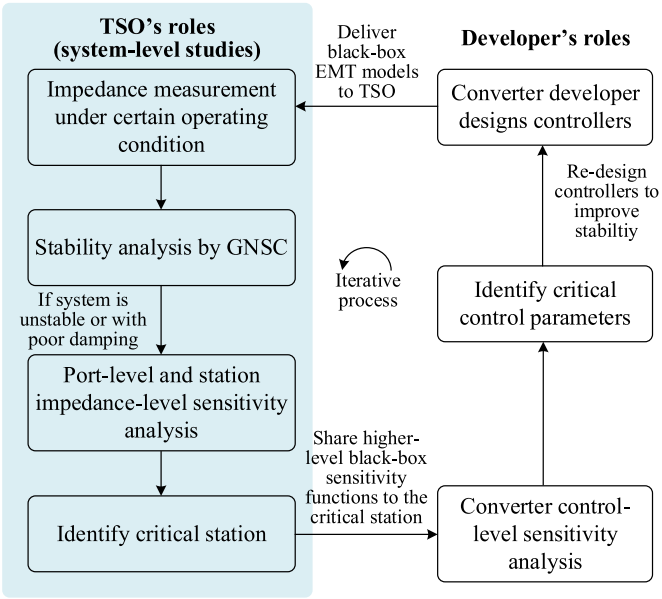

FIGURE 5. Flowchart of using the multi-level sensitivity analysis approach for system-level interoperability studies.

At the station impedance level, the normalized sensitivity functions of critical eigenloci with respect to different station impedances can be compared. In the critical frequency range, the highest sensitivity magnitude indicates which station takes a dominant role in the system stability or instability.

At the converter control level, the normalized sensitivity functions of critical eigenloci with respect to different control parameters can also be compared, indicating which control parameters affect the stability or instability significantly.

It is noted that the sensitivity analysis is only necessary when the system is unstable, or close to instability with poor damping, i.e., there exist eigenloci of $\mathbf{L}(\omega)$ that are close to $(-1, 0)$. In addition, the sensitivity analysis only indicates which element/subsystem influences the stability most. It does not mean that this is the exact element/subsystem that destabilizes the system, since the system stability shall be determined by all the elements or subsystems, not by only one. However, the sensitivity analysis result can be very useful for system-level design. If the most sensitive element/subsystem can be found, tuning or designing the sensible element/subsystem will have a significant impact on the stability improvement, thus the sensitivity analysis result can effectively help the system-level design and optimization.

To elaborate the application of this approach for system-level interoperability studies in multi-vendor projects, a flowchart is provided in Fig. 5. It can be seen that this approach only relies on sharing information based on black-box forms. On one hand, the TSO can collect black-box EMT models from converter developers to conduct system-level stability analysis. On the other hand, whenever the system is exposed to risks of instability or poor damping, the TSO may share the higher-level black-box sensitivity functions to the critical (most sensitive) station if needed, in order to help the converter developer redesign their converter controllers to improve the overall system stability.

E. COMPARISON WITH EXISTING SENSITIVITY METHODS

The differences between the proposed method with the existing sensitivity methods are discussed from their principles to show the advantages of the proposed method for black-box systems.

1) COMPARISON WITH CLASSICAL MODAL-BASED SENSITIVITY METHOD

To compare the proposed frequency-domain sensitivity method with the classical modal-based sensitivity method, Fig. 6 provides the procedures for their applications to a black-box system. Since the state-space model is unknown for the black-box system, the classical method is based on the identification of transfer function models and pole analysis. Due to different principles of the methods, the two approaches follow different procedures. The involved calculation methods in each step are described in different colored text beside the flowchart. It can be found that

- The proposed frequency-domain sensitivity method only involves matrix calculation and partial derivative, which is relatively simper.
- The classical modal-based sensitivity method involves more complex steps, including the system identification of s-domain transfer functions and pole calculation by solving high-order algebraic equations. The system identification needs to be carefully designed to avoid under- or over-fitting problems. The pole calculation also requires solving high-order algebraic equations, which is also not so easy as only using matrix calculation in the proposed method.

Therefore, the proposed method provides an easier way to analyze black-box systems, as it does not require solving the system oscillation modes.

2) COMPARISON WITH DETERMINANT-BASED SENSITIVITY METHOD

The determinant-based sensitivity method also utilizes frequency-domain sensitivity function; however, it considers the stability and sensitivity based on the determinant of the return difference, i.e., $\det(\mathbf{F}(\omega))$. Since $\mathbf{F}(\omega) = \mathbf{E} + \mathbf{L}(\omega)$, it holds that

$$\det\left(\mathbf{F}\left(\omega\right)\right) = \prod_{i}\left(1 + \lambda_i\left(\omega\right)\right) \tag{15}$$

where $\lambda_i(\omega)$ for all i are the eigenvalues of $\mathbf{L}(\omega)$. Apparently, $\det(\mathbf{F}(\omega))$ is a more complex function than any $\lambda_i(\omega)$, since it considers the multiplication of $(1+ \lambda_i(\omega))$ for all i. Therefore, calculating the sensitivity functions of $\det(\mathbf{F}(\omega))$ is more complex than calculating the sensitivity functions of only one eigenlocus $\lambda_i(\omega)$.

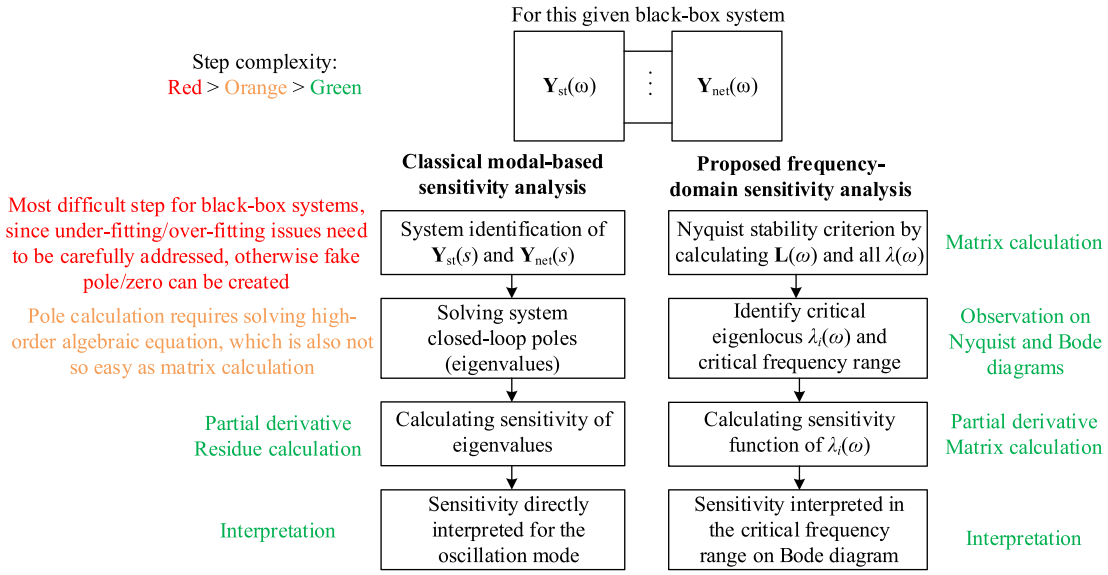

FIGURE 6. Comparison of the proposed and the classical sensitivity methods for a black-box system.

TABLE 1. Main Circuit Parameters of the MMC Station

Symbol	Description	Value
V_{gac}	Rated ac voltage at grid side (Line to line, RMS)	380 kV
V_{cac}	Rated ac voltage at converter side (Line to line, RMS)	273 kV
L_k	Leakage inductance of the transformer	0.1 p.u.
V_{dc}	Rated DC voltage	525 kV
S_n	Power rating	1050 MVA
L_{arm}	Arm inductance	15 mH
L_{dc}	DC smooth inductance	30 mH
C_{sm}	Capacitance of submodule	6 mF
N_{sm}	Number of submodules in each arm	276

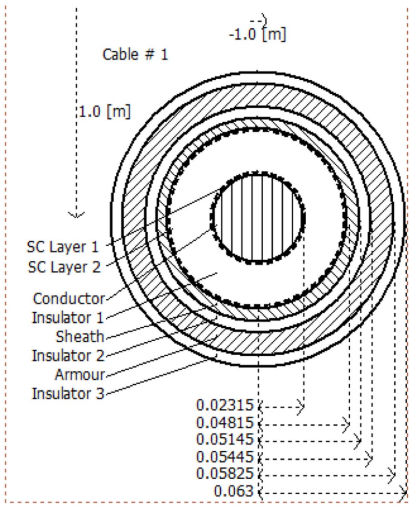

FIGURE 7. Geometrical parameters of DC cables, based on which their electrical parameters can be computed in PSCAD.

IV. CASE STUDIES

Two case studies are carried out for the stability and sensitivity analysis of the system in Fig. 1. Since this work assumes the converters are black-box systems and mainly focuses on the system-level stability studies for TSOs, as shown in the left column of Fig. 5, only port-level and station impedance-level sensitivity analyses are performed.

A. IMPEDANCE MEASUREMENT

Since the MMC stations are black-box systems with unknown control parameters, only the electric circuit parameters are provided in Table 1. The DC cables are represented by frequency-dependent phase models in PSCAD, whose electrical parameters are internally computed in PSCAD based on their geometrical parameters, as shown in Fig. 7. The impedance models of the MMC-HVDC stations and the DC cables are all measured in PSCAD by the PSCAD-compatible software toolbox developed in [17].

The detailed measurement settings for using the automated impedance measurement software toolbox can be found in [16], [17], including frequency range of interest, frequency resolution, simulation time step, etc., as shown in Fig. 8.

For the MMC station, since each station always adopts the same control for positive and negative poles, meaning that, $Z_{p,m} = Z_{n,m}$, only $Z_{p,m}$ is measured. Then, the admittance matrix of each station is calculated by (2).

For the DC cable, its six-port cable admittance matrix can be solved by the superposition principle based on six measurements with a perturbation source at each port. Then, the

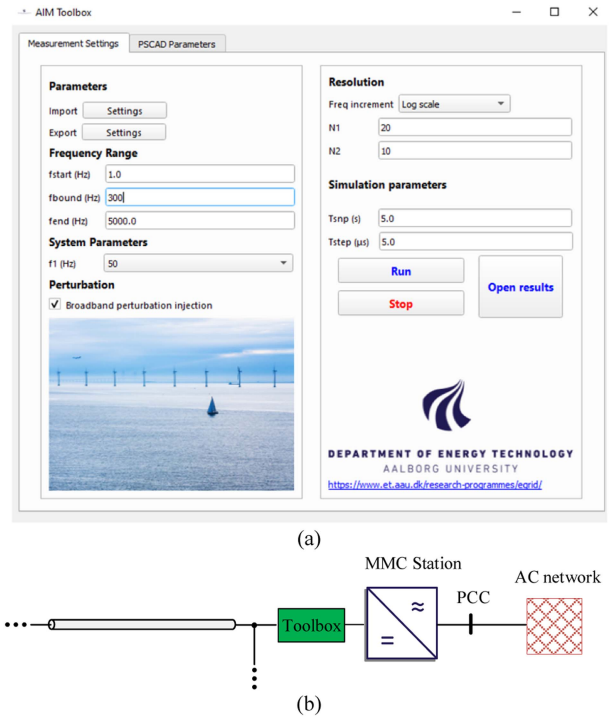

FIGURE 8. **(a) Graphical user interface (GUI) of the toolbox. (b) Toolbox connection for dc impedance measurement of the MMC.**

admittance matrix of the entire DC network can be calculated by (3).

The measured impedance data has been submitted to IEEE DataPort [24] for the stability validation, since the converter control parameters cannot be disclosed. Then, the stability and sensitivity can be analyzed based on the measured impedance data. The stability and sensitivity analyses are implemented by pre-programming in MATLAB, and the scripts only run less than 2 seconds to deal with the impedance data and obtain the Nyquist and Bode diagrams, which is almost negligible compared with the frequency scans in EMT simulations. The analysis results are compared with the EMT simulations for validation.

B. CASE I – UNSTABLE CASE

First, an unstable case is studied. The stability analysis results are provided in Fig. 9. Fig. 9(a) shows the Bode diagram of $\det(\mathbf{F}(\omega))$. It can be seen that at all the resonant peaks, the phase is decreasing, indicating that $\det(\mathbf{F}(\omega))$ has none RHP poles [25]. Thus, $P = 0$. Fig. 9(b) shows the Nyquist diagrams of all the eigenloci of $\mathbf{L}(\omega)$ within the positive frequency range. Since $\mathbf{L}(\omega)$ has the rank of 8, only eight non-zero eigenloci are plotted. It can be seen that $\lambda_1(\omega)$ and $\lambda_2(\omega)$ encircle $(-1, 0)$ clockwise two times in total. If the negative frequency range is considered, the total number of clockwise encirclements is four, i.e., $N = -4$. Thus, the system is unstable.

Fig. 10 provides the EMT simulation results of Case I. Oscillations are observed in the time-domain waveforms. From

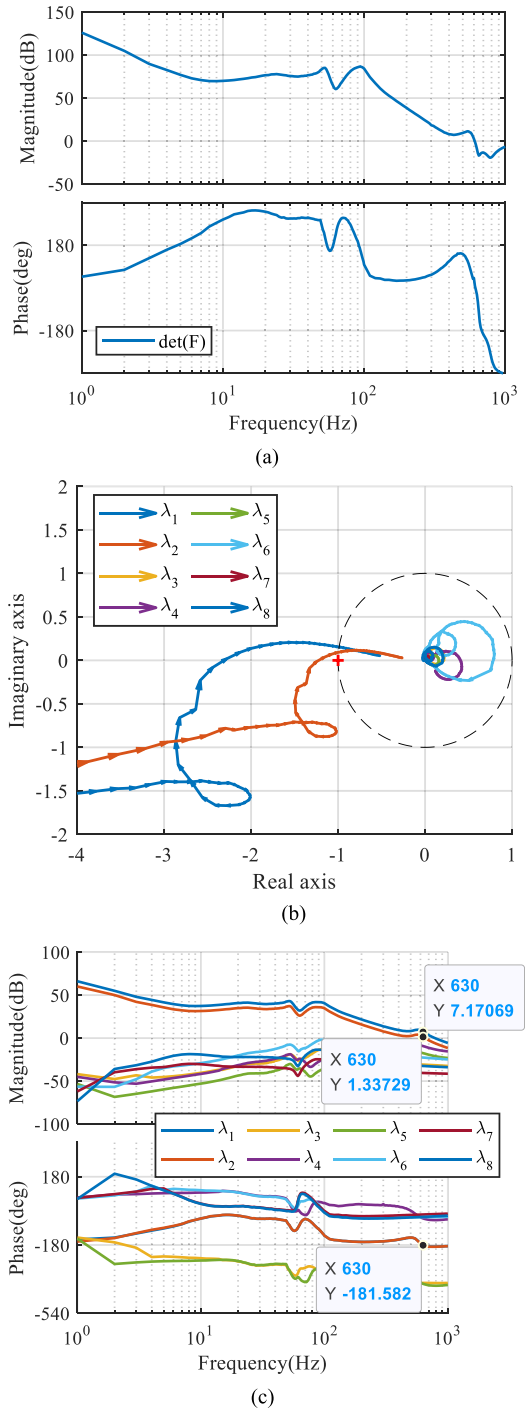

FIGURE 9. **Stability analysis for Case I. (a) Bode diagram of det(F(ω)); (b) Nyquist diagrams of $\lambda_i(\omega)$; (c) Bode diagrams of $\lambda_i(\omega)$.**

the power waveforms, it is seen that the oscillations are mainly present at the DC side, indicating that the instability is induced from DC system interactions. The discrete Fourier analysis of the DC-link voltage in Fig. 10(b) indicates an oscillation frequency around 630 Hz, which closely agrees with the phase crossover frequency of 180° shown in the Bode diagram

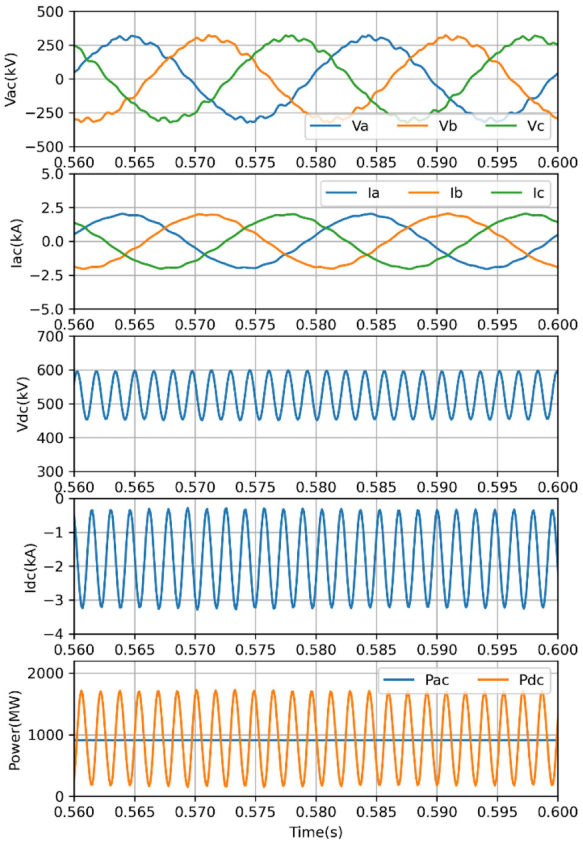

FIGURE 10. EMT simulation results for Case I. (a) Time-domain waveforms; (b) Discrete Fourier analysis of the DC-link voltage.

of Fig. 9(c). The accuracy of the stability analysis is thus verified.

Since the DC system is unstable, the sensitivity analysis is further conducted. Both $\lambda_1(\omega)$ and $\lambda_2(\omega)$ are close to $(-1, 0)$, thus they are the critical eigenloci. The Bode diagrams of the eigenloci in Fig. 9(c) also indicate that the critical frequency range should be around 630 Hz.

The port-level sensitivity analysis is conducted first. The port participation functions of $\lambda_1(\omega)$ and $\lambda_2(\omega)$ are calculated and their magnitude responses are compared in Fig. 11. Fig. 11(a) plots the first column of (10) for $\lambda_1(\omega)$, and

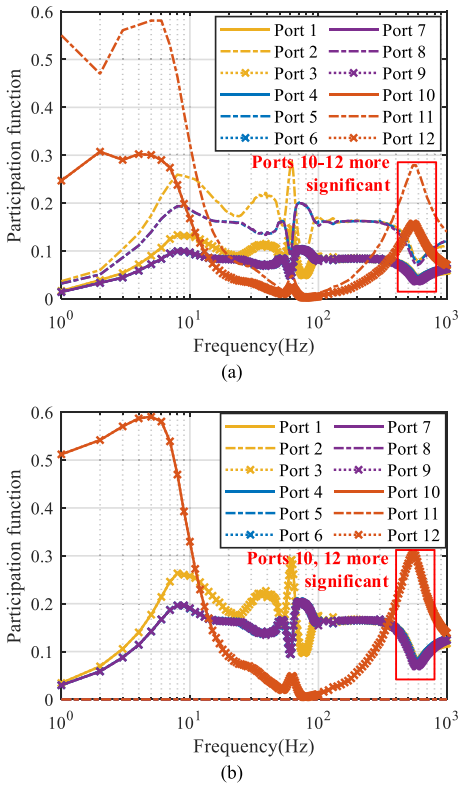

FIGURE 11. Port participation analysis of λ_1 and λ_2 for Case I. (a) Participation analysis of λ_1; (b) Participation analysis of λ_2.

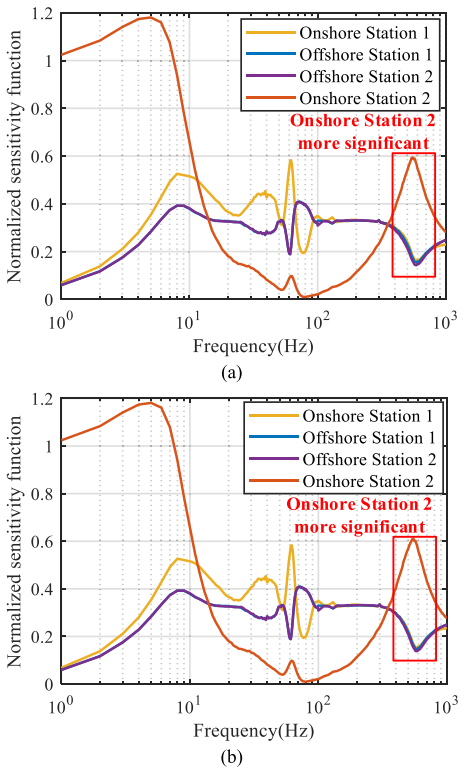

FIGURE 12. Station impedance-level sensitivity analysis of λ_1 and λ_2 for Case I. (a) Sensitivity analysis of λ_1; (b) Sensitivity analysis of λ_2.

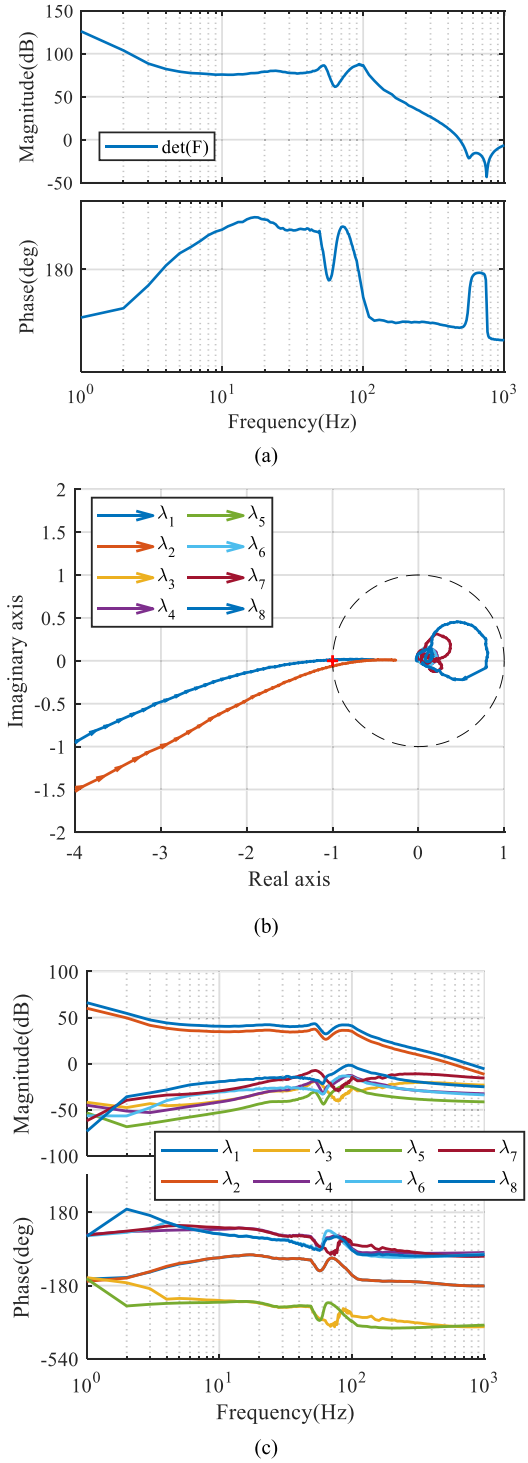

FIGURE 13. Stability analysis for Case II. (a) Bode diagram of det(F(ω)); (b) Nyquist diagrams of $\lambda_i(\omega)$; (c) Bode diagrams of $\lambda_i(\omega)$.

Fig. 11(b) plots the second column of (10) for $\lambda_2(\omega)$, where each line represents the participation of one port. It can be seen that in the critical frequency range, as marked in the red box, the sensitivity functions with respect to Ports 10-12 have larger magnitudes than others. These ports are associated with the Onshore Station 2. It is thus implied that the instability is more sensitive to the Onshore Station 2.

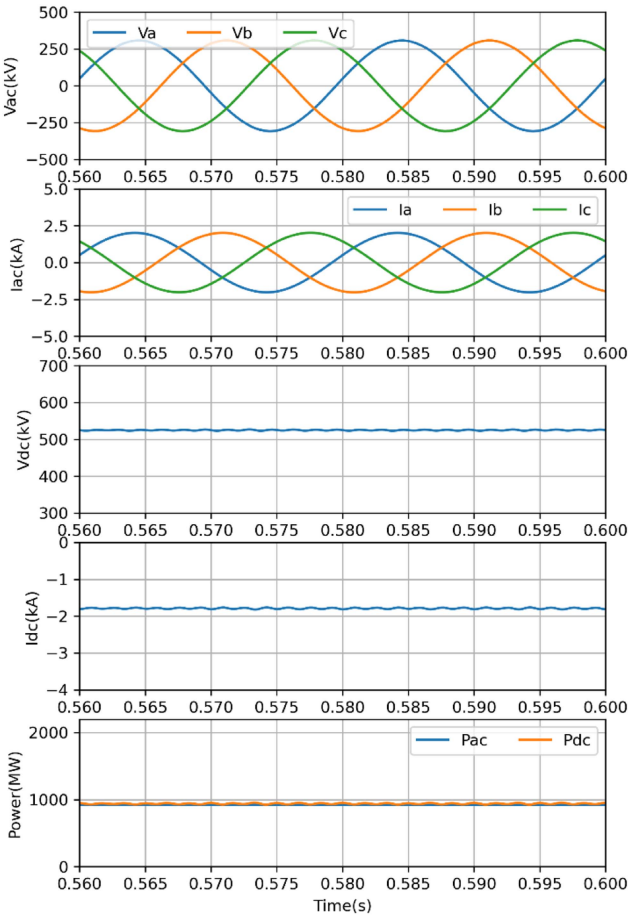

FIGURE 14. EMT simulation results for Case II.

The station impedance-level sensitivity is further analyzed. Since each MMC station has the same positive-pole and negative-pole impedances, the normalized sensitivity functions of $\lambda_1(\omega)$ and $\lambda_2(\omega)$ are only calculated with respect to the positive-pole impedance, whose magnitudes are compared in Fig. 12. Fig. 12(a) is calculated by (13) for $\lambda_1(\omega)$, and Fig. 12(b) is calculated by (13) for $\lambda_2(\omega)$, where each line represents the sensitivity function for one station impedance. It is seen that in the critical frequency range, as marked in the red box, the Onshore Station 2 impedance has the largest sensitivity magnitude. It is implied that the instability is most sensitive to the Onshore Station 2, which agrees with the conclusion from port-level sensitivity analysis.

C. CASE II – CRITICALLY UNSTABLE CASE

The sensitivity analysis of Case I has indicated that Onshore Station 2 affects the stability most significantly. Thus, Case II is further analyzed by slightly tuning the control parameters of the Onshore Station 2.

The stability analysis is provided in Fig. 13. It can be seen that now only λ_1 critically encircles $(-1, 0)$, which implies the stability has been improved compared with Fig. 9 by changing

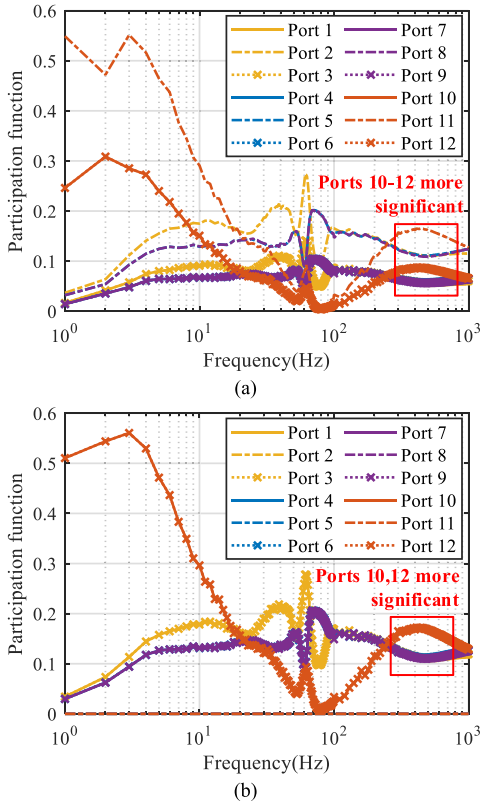

FIGURE 15. Port participation analysis of λ_1 and λ_2 for Case II. (a) Participation analysis of λ_1; (b) Participation analysis of λ_2.

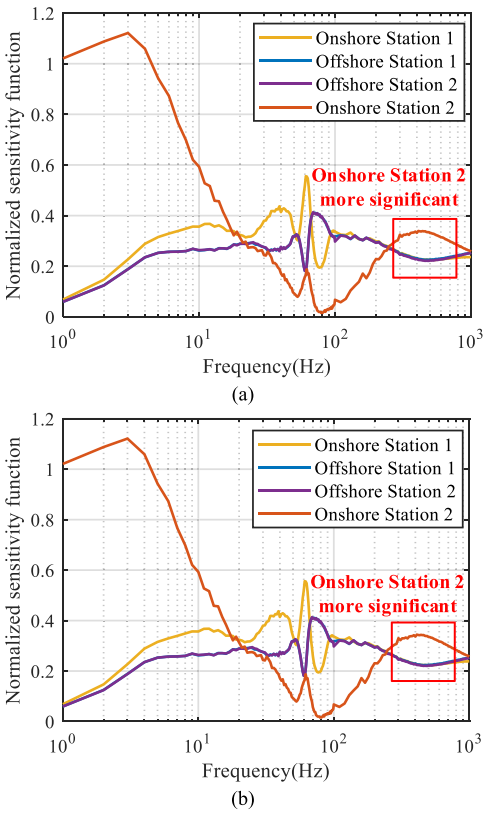

FIGURE 16. Station impedance-level sensitivity analysis of λ_1 and λ_2 for Case II. (a) Sensitivity analysis of λ_1; (b) Sensitivity analysis of λ_2.

the control parameters of the Onshore Station 2. This also verifies the sensitivity analysis of Case I. The EMT simulation results are provided in Fig. 14, where the oscillations have been damped significantly compared with Case I. Only small oscillations in DC voltage and current are observed, since the system is under a critically unstable condition. The sensitivity analyses at the port level and station impedance level are shown in Figs. 15 and 16, which also show similar results to Case I, indicating that the stability is more sensitive to the Onshore Station 2.

V. CONCLUSION AND PROSPECTS

A multi-level sensitivity analysis approach has been developed to analyze the stability of multi-terminal HVDC systems. This approach is derived based on the frequency-domain sensitivity theory, which is thus readily applicable for black-box systems with only impedance representations. It can well address the challenge of converter interoperability among multi-vendor projects.

The proposed approach allows for sensitivity analysis from the system level to converter control level, which provides further insights into the system stability analysis and design. Its potential applications may include:

- Port-level and station impedance-level sensitivity can help TSOs perform the system-level stability analysis and identify the root cause (meaning the most sensitive station/converter) of potential instability.
- The system-level black-box sensitivity functions can also be shared by TSOs and transferred down to the converter developers to help them further conduct the control-level sensitivity analysis and robust controller design.

APPENDIX

A. PROOF OF (9)

Based on the eigenvalue and eigenvector of $\mathbf{L}(\omega)$, there exists

$$\begin{aligned}&\mathbf{L}(\omega)\,\mathbf{v}_i(\omega)=\lambda_i(\omega)\,\mathbf{v}_i(\omega)\\&\text{where } \lambda_i(\omega) \text{ is the } i\text{-th eigenvalue}\\&\qquad \mathbf{v}_i(\omega) \text{ is the } i\text{-th right eigenvector}\end{aligned}\tag{A1}$$

Differentiating (A1) with respect to $l_{jk}(\omega)$, i.e., the j-th row and k-th column element of $\mathbf{L}(\omega)$, it yields that

$$\begin{aligned}&\frac{\partial \mathbf{L}(\omega)}{\partial l_{jk}(\omega)}\mathbf{v}_i(\omega)+\mathbf{L}(\omega)\frac{\partial \mathbf{v}_i(\omega)}{\partial l_{jk}(\omega)}\\&\quad=\frac{\partial \lambda_i(\omega)}{\partial l_{jk}(\omega)}\mathbf{v}_i(\omega)+\lambda_i(\omega)\frac{\partial \mathbf{v}_i(\omega)}{\partial l_{jk}(\omega)}\end{aligned}\tag{A2}$$

Multiplying both sides of (A2) with the left eigenvector $\mathbf{w}_i(\omega)$ and reformulating the equation, it can be derived that

$$\frac{\partial \lambda_i(\omega)}{\partial l_{jk}(\omega)}\mathbf{w}_i(\omega)\,\mathbf{v}_i(\omega)=\mathbf{w}_i(\omega)\frac{\partial \mathbf{L}(\omega)}{\partial l_{jk}(\omega)}\mathbf{v}_i(\omega)$$

$$+\mathbf{w}_i(\omega)\left(\mathbf{L}(\omega)-\lambda_i(\omega)\mathbf{E}\right)\frac{\partial \mathbf{v}_i(\omega)}{\partial l_{jk}(\omega)} \tag{A3}$$

Since $\mathbf{w}_i(\omega)\mathbf{v}_i(\omega)=1$ and $\mathbf{w}_i(\omega)(\mathbf{L}(\omega)-\lambda_i(\omega)\mathbf{E})=0$, (A3) can be simplified as

$$\frac{\partial \lambda_i(\omega)}{\partial l_{jk}(\omega)}=\mathbf{w}_i(\omega)\frac{\partial \mathbf{L}(\omega)}{\partial l_{jk}(\omega)}\mathbf{v}_i(\omega) \tag{A4}$$

Since all the elements of $\frac{\partial \mathbf{L}(\omega)}{\partial l_{jk}(\omega)}$ are zero, except for the element in the j-th row and k-th column which is equal to 1, (9) can be further derived.

B. PROOF OF (11)

According to the sensitivity definition and partial derivative, it can be derived that

$$\begin{aligned}\mathbf{S}^{\mathbf{L}}_{Z_{p/n,m}}(\omega) &:= \frac{\partial \mathbf{L}(\omega)}{\partial Z_{p/n,m}(\omega)}=\frac{\partial\left(\mathbf{Y}_{\mathrm{st}}(\omega)\mathbf{Z}_{\mathrm{net}}(\omega)\right)}{\partial Z_{p/n,m}(\omega)}\\ &=\frac{\partial \mathbf{Y}_{\mathrm{st}}(\omega)}{\partial Z_{p/n,m}(\omega)}\mathbf{Z}_{\mathrm{net}}(\omega)\\ &\quad+\mathbf{Y}_{\mathrm{st}}(\omega)\frac{\partial \mathbf{Z}_{\mathrm{net}}(\omega)}{\partial Z_{p/n,m}(\omega)}\end{aligned} \tag{A5}$$

Since $\mathbf{Z}_{\mathrm{net}}(\omega)$ is the passive network impedance, which is independent of $Z_{p/n,m}(\omega)$, there exists

$$\frac{\partial \mathbf{Z}_{\mathrm{net}}(\omega)}{\partial Z_{p/n,m}(\omega)}=\mathbf{O} \text{ where } \mathbf{O} \text{ is a zero matrix} \tag{A6}$$

Therefore, it can be further derived that

$$\begin{aligned}\mathbf{S}^{\mathbf{L}}_{Z_{p/n,m}}(\omega) &:= \frac{\partial \mathbf{L}(\omega)}{\partial Z_{p/n,m}(\omega)}=\frac{\partial \mathbf{Y}_{\mathrm{st}}(\omega)}{\partial Z_{p/n,m}(\omega)}\mathbf{Z}_{\mathrm{net}}(\omega)\\ &=\frac{\partial\begin{bmatrix}\mathbf{Y}_1(\omega) & & \\ & \ddots & \\ & & \mathbf{Y}_k(\omega) & \\ & & & \ddots\end{bmatrix}}{\partial Z_{p/n,m}(\omega)}\mathbf{Z}_{\mathrm{net}}(\omega)\\ &=\begin{bmatrix}\frac{\partial \mathbf{Y}_1(\omega)}{\partial Z_{p/n,m}(\omega)} & & \\ & \ddots & \\ & & \frac{\partial \mathbf{Y}_k(\omega)}{\partial Z_{p/n,m}(\omega)} & \\ & & & \ddots\end{bmatrix}\mathbf{Z}_{\mathrm{net}}(\omega)\end{aligned} \tag{A7}$$

where $\frac{\partial \mathbf{Y}_k(\omega)}{\partial Z_{p/n,m}(\omega)}=\mathbf{O}$ for $k\neq m$, since $\mathbf{Y}_k(\omega)$ is irrelevant to $Z_{p/n,m}(\omega)$

$\frac{\partial \mathbf{Y}_m(\omega)}{\partial Z_{p/n,m}(\omega)}\neq\mathbf{O}$, which can be derived according to (2)

To derive $\frac{\partial \mathbf{Y}_m(\omega)}{\partial Z_{p/n,m}(\omega)}$, assuming $Z_{p,m}=Z_{n,m}$ (this holds since the positive and negative poles of an HVDC converter are usually designed with the same controls and dynamics), (2) can be expressed as

$$\mathbf{Y}_m(\omega)=\begin{bmatrix}\frac{1}{Z_{p,m}(\omega)} & -\frac{1}{Z_{p,m}(\omega)} & \\ -\frac{1}{Z_{p,m}(\omega)} & \frac{2}{Z_{p,m}(\omega)} & -\frac{1}{Z_{p,m}(\omega)}\\ & -\frac{1}{Z_{p,m}(\omega)} & \frac{1}{Z_{p,m}(\omega)}\end{bmatrix} \tag{A8}$$

Thus, the partial derivative can be derived as

$$\frac{\partial \mathbf{Y}_m(\omega)}{\partial Z_{p,m}(\omega)}=\begin{bmatrix}-\frac{1}{Z^2_{p,m}(\omega)} & \frac{1}{Z^2_{p,m}(\omega)} & \\ \frac{1}{Z^2_{p,m}(\omega)} & -\frac{2}{Z^2_{p,m}(\omega)} & \frac{1}{Z^2_{p,m}(\omega)}\\ & \frac{1}{Z^2_{p,m}(\omega)} & -\frac{1}{Z^2_{p,m}(\omega)}\end{bmatrix} \tag{A9}$$

REFERENCES

[1] North Sea Wind Power Hub Consortium, "Unlocking the North Sea as a green powerplant," 2022. [Online]. Available: https://northseawindpowerhub.eu/sites/northseawindpowerhub.eu/files/media/document/NSWPH_Insights_15.09.2022_CMYK_without%20cropmarks.pdf

[2] C. Buchhagen, C. Rauscher, A. Menze, and J. Jung, "BorWin1 - first experiences with harmonic interactions in converter dominated grids," in *Proc. Int. ETG Congr. Die Energiewende - Blueprints New Energy Age*, 2015, pp. 1–7.

[3] H. Saad, Y. Fillion, S. Deschanvres, Y. Vernay, and S. Dennetière, "On resonances and harmonics in HVDC-MMC station connected to AC grid," *IEEE Trans. Power Del.*, vol. 32, no. 3, pp. 1565–1573, Jun. 2017.

[4] ENTSO-E, "Position on offshore development – interoperability," Jan. 2021. [Online]. Available: https://eepublicdownloads.entsoe.eu/clean-documents/Publications/Position%20papers%20and%20reports/210125_Offshore%20Development_Interoperability.pdf

[5] ENTSO-E, T&D Europe, WindEurope, "Workstream for the development of multi-vendor HVDC systems and other power electronics interfaced devices," Mar. 2021. [Online]. Available: https://eepublicdownloads.azureedge.net/clean-documents/RDC%20documents/210505%20Multi-Vendor-HVDC-workstream.pdf

[6] S. Liu, Z. Xu, W. Hua, G. Tang, and Y. Xue, "Electromechanical transient modeling of modular multilevel converter based multi-terminal HVDC systems," *IEEE Trans. Power Syst.*, vol. 29, no. 1, pp. 72–83, Jan. 2014.

[7] J. Lyu, X. Cai, and M. Molinas, "Frequency domain stability analysis of MMC-based HVdc for wind farm integration," *IEEE J. Emerg. Sel. Topics Power Electron.*, vol. 4, no. 1, pp. 141–151, Mar. 2016.

[8] G. Pinares and M. Bongiorno, "Modeling and analysis of VSC-based HVDC systems for DC network stability studies," *IEEE Trans. Power Del.*, vol. 31, no. 2, pp. 848–856, Apr. 2016.

[9] T. Li, A. M. Gole, and C. Zhao, "Harmonic instability in MMC-HVDC converters resulting from internal dynamics," *IEEE Trans. Power Del.*, vol. 31, no. 4, pp. 1738–1747, Aug. 2016.

[10] H. Wu, X. Wang, and Ł. H. Kocewiak, "Impedance-based stability analysis of voltage-controlled MMCs feeding linear AC systems," *IEEE J. Emerg. Sel. Topics Power Electron.*, vol. 8, no. 4, pp. 4060–4074, Dec. 2020.

[11] X. Wang and F. Blaabjerg, "Harmonic stability in power electronic-based power systems: Concept, modeling, and analysis," *IEEE Trans. Smart Grid*, vol. 10, no. 3, pp. 2858–2870, May 2019.

[12] Y. Zhan, X. Xie, and Y. Wang, "Impedance network model based modal observability and controllability analysis for renewable integrated power systems," *IEEE Trans. Power Del.*, vol. 36, no. 4, pp. 2025–2034, Aug. 2021.

[13] Y. Zhu, Y. Gu, Y. Li, and T. Green, "Participation analysis in impedance models: The grey-box approach for power system stability," *IEEE Trans. Power Syst.*, vol. 37, no. 1, pp. 343–353, Jan. 2022.

[14] H. Zhang, X. Wang, M. Mehrabankhomartash, M. G. Saeedifard, Y. Meng, and X. Wang, "Harmonic stability assessment of multi-terminal DC (MTDC) systems based on the hybrid AC/DC admittance model and determinant-based GNC," *IEEE Trans. Power Electron.*, vol. 37, no. 2, pp. 1653–1665, Feb. 2022.

[15] Y. Liao, X. Wang, and X. Wang, "Frequency-domain participation analysis for electronic power systems," *IEEE Trans. Power Electron.*, vol. 37, no. 3, pp. 2531–2537, Mar. 2022.
[16] D. Yang, X. Wang, M. Ndreko, W. Winter, R. Juhlin, and A. Krontiris, "Automation of impedance measurement for harmonic stability assessment of MMC-HVDC systems," in *Proc. 18th Wind Integration Workshop*, 2019, pp. 1–6.
[17] H. Wu, X. Wang, Y. Liao, M. Ndreko, R. Dimitrovski, and W. Winter, "Development of the toolbox for AC/DC impedance matrix measurement of MTDC system," in *Proc. 20th Wind Integration Workshop*, 2021, pp. 442–448.
[18] Y. Li et al., "Stability analysis and location optimization method for multiconverter power systems based on nodal admittance matrix," *IEEE J. Emerg. Sel. Topics Power Electron.*, vol. 9, no. 1, pp. 529–538, Feb. 2021.
[19] D. Sun, H. Liu, and M. Gong, "A stability analysis tool for bulk power systems using black-box models of inverter-based resources," in *Proc. IEEE Ind. Appl. Soc. Annu. Meeting*, 2022, pp. 1–6.
[20] A. MacFarlane, "Return-difference and return-ratio matrices and their use in analysis and design of multivariable feedback control systems," in *Proc. Inst. Elect. Engineers*, vol. 117, no. 10, pp. 2037–2049, 1970.
[21] G. F. Franklin, J. D. Powell, and A. Emami-Naeini, *Feedback Control of Dynamic Systems*. London, U.K.: Pearson Educ. Limited, 2015.
[22] P. M. Frank, *Introduction to System Sensitivity Theory*. New York, NY, USA: Academic, 1978.
[23] P. Kundur, *Power System Stability and Control*. New York, NY, USA: McGraw-hill. 1994.
[24] Y. Liao, H. Wu, X. Wang, M. Ndreko, R. Dimitrovski, and W. Winter, "Impedance data for a four-terminal HVDC system," IEEE DataPort, Jan. 2023, doi: 10.21227/4mac-b212.
[25] Y. Liao and X. Wang, "Impedance-based stability analysis for interconnected converter systems with open-loop RHP poles," *IEEE Trans. Power Electron.*, vol. 35, no. 4, pp. 4388–4397, Apr. 2020.

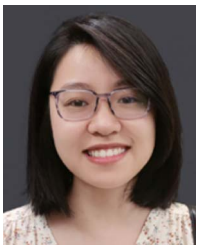

YICHENG LIAO (Member, IEEE) received the B.S. and M.S. degrees in electrical engineering from Southwest Jiaotong University, Chengdu, China, in 2015 and 2018, respectively, and the Ph.D. degree in energy technology from Aalborg University, Aalborg, Denmark, in 2021.

In July 2017, she was a Visiting Student with the Ecole Polytechnique and French National Institute for Research in Digital Science and Technology, Paris, France. From 2018 to July 2021, she was with AAU Energy, Aalborg University, as a Research Assistant and later on a Postdoc. From August 2021 to December 2021, she was a Postdoc with the School of Electrical Engineering and Computer Science, KTH Royal Institute of Technology, Stockholm, Sweden. Since 2022, she has been a Power System Engineer with the Department of Electrical System Design, Energinet, Fredericia, Denmark. She is also a Member of the Cigre working group C4.71. Her research interests include the modeling, stability analysis, and control of power electronics-based power systems.

Dr. Liao was selected as the 2020 Outstanding Reviewer of IEEE TRANSACTIONS ON POWER ELECTRONICS and the 2020 Star Reviewer of the IEEE JOURNAL OF EMERGING AND SELECTED TOPICS IN POWER ELECTRONICS. She was the recipient of the 2020 Top Download Paper Award in IEEE OPEN JOURNAL OF THE INDUSTRIAL ELECTRONICS SOCIETY and 2021 Ph.D. Thesis Talk Award in IEEE Power Electronics Society.

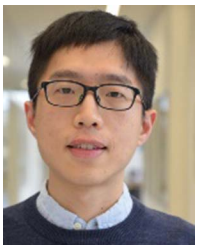

HENG WU (Member, IEEE) received the B.S. and M.S. degrees in electrical engineering from the Nanjing University of Aeronautics and Astronautics, Nanjing, China, in 2012 and 2015, respectively, and the Ph.D. degree in electrical engineering from Aalborg University, Aalborg, Denmark, in 2020. He is currently an Assistant Professor with AAU Energy, Aalborg University.

From 2015 to 2017, he was an Electrical Engineer with NR Electric Co., Ltd, Nanjing, China. He was a Guest Researcher with Ørsted Wind Power, Fredericia, Denmark, in 2018, and Bundeswehr University, Munich, Germany, in 2019. From 2020 to 2021, he was a Postdoctoral Researcher with Aalborg University, Aalborg, Denmark. He is the Co-Chair of IEEE Task Force on Frequency-domain Modeling and Dynamic Analysis of HVDC and FACTS, a Member of the technical committee (TC) of the European Academy of Wind Energy, Member of GB grid forming best practice expert group formed by national grid ESO, U.K., Member of Cigre working group B4.85 and B4/C4.93, and Steering Committee Member of Cigre next generation network, Denmark. His research interests include the modeling and stability analysis of the power electronic based power systems. In 2019, he is identified as world's top 2% scientist by Stanford University, Stanford, CA, USA. He was the recipient of the 2019 Outstanding Reviewer Award of the IEEE TRANSACTIONS ON POWER ELECTRONICS and the 2021 Star Reviewer Award of the IEEE JOURNAL OF EMERGING AND SELECTED TOPICS IN POWER ELECTRONICS.

XIONGFEI WANG (Fellow, IEEE) received the B.S. degree in electrical engineering from Yanshan University, Qinhuangdao, China, in 2006, the M.S. degree in electrical engineering from the Harbin Institute of Technology, Harbin, China, in 2008, and the Ph.D. degree in energy technology from Aalborg University, Aalborg, Denmark, in 2013.

From 2009 to 2022, he was with Aalborg University, where he became an Assistant Professor in 2014, an Associate Professor in 2016, a Professor and Leader of Electronic Power Grid (eGRID) Research Group in 2018. Since 2022, he has been a Professor with the KTH Royal Institute of Technology, Stockholm, Sweden. His research interests include modeling and control of power electronic converters and systems, stability and power quality of power-electronics-dominated power systems, and high-power converters.

Dr. Wang is the Co-Editor-in-Chief of the IEEE TRANSACTIONS ON POWER ELECTRONICS and an Associate Editor for the IEEE JOURNAL OF EMERGING AND SELECTED TOPICS IN POWER ELECTRONICS. He was the recipient of ten IEEE Prize Paper Awards, 2016 AAU Talent for Future Research Leaders, 2018 Richard M. Bass Outstanding Young Power Electronics Engineer Award, 2019 IEEE PELS Sustainable Energy Systems Technical Achievement Award, 2020 JESTPE Star Associate Editor Award, and 2022 Isao Takahashi Power Electronics Award.

MARIO NDREKO received the Ph.D. degree in electrical engineering from the Delft University of Technology, Delft, The Netherlands, in 2017, on the topic of grid connection code compliance optimisation for offshore wind power plants with HVDC transmission.

Since 2017, he has been with TenneT TSO GmbH in Germany first at the Asset Management - Grid Planning Department and then at the Energy System Planning Department in the role of HVDC systems and Connection Network Codes Specialist. Between 2017 and 2021, he was a Member of the ENTSO-E working group future power system stability in the Research, Development and Innovation Committee of ENTSO-E. During this period, he contributed to EU Funded Migrate project with focus on the development of grid forming control concepts for power converters. Since 2021, he has been the Convener of the ENTSO-E Group connection network codes. In addition, he is responsible within TenneT for the global system integrity process, which focuses on the interaction studies and interoperability of AC-DC transmission systems as well multiterminal HVDC grids. He is the author of various journal and conference contributions on the topic of grid connection studies for HVDC systems and wind power park modules.

ROBERT DIMITROVSKI received the M.Sc. degree in electrical power engineering from the Brandenburg University of Technology, Cottbus, Germany, in 2011, and the Ph.D. degree in electrical power engineering from the Friedrich-Alexander-Universität Erlangen-Nürnberg, Germany, in 2021. From 2011 to 2014, he was with Siemens AG, Germany, Smart Grid Division, where he was responsible for the real-time testing of various SIPROTEC relay protection devices.

Since 2020, he has been with TenneT TSO GmbH with Energy System Planning / Grid Analysis department. Within TenneT, he is responsible for the EU Funded Project HVDC-Wise. He is involved in various projects related to analysis of electrical power systems and the development of collaborative open-source energy system simulation tools. He is also a Member of the ENTSO-e group Security and Operations of tomorrow, where he is leading the Grid Assessment workstream and a Member of the Cigre working group C4/B4.52.

WILHELM WINTER received the M.S. (Dipl.-Ing.) and Ph.D. (Dr.-Ing.) degrees in power engineering from the Technical University of Berlin, Berlin, Germany, in 1995 and 1998, respectively.

From 1995 to 2002, he was with Siemens, System Planning Department responsible for Modal Analysis, HVDC, and FACTS. He was involved in large system studies, including stability calculations, HVDC, and FACTS optimizations, modal analysis, transient phenomena, real-time simulation, and renewable energy systems. He was responsible for the development of the NETOMAC Eigenvalue Analysis Program. In 2002, he changed to EON Netz GmbH setting up the new workstream for grid stability. He was responsible for drafting the E.ON Netz Netzanschlussregeln for renewable generation. He was involved in large European system studies, coordinating the European Wind Integration study in 2007 and umbrella in 2010. Since 2010, he has been with TenneT TSO GmbH and was appointed to Expert on HVDC Overlay Grid Design and System Security in 2012, leading the expert team for HVDC & Connection Codes. In parallel, he was appointed to the ENTSO-E convener of the network code HVDC drafting team. Since 2020, he has been appointed for the lead of Electrical System Design in Energy System Planning.